The Global Seismographic Network Reveals Atmospherically Coupled Normal Modes excited by the 2022 Hunga Tonga Eruption

Ringler, A. T.[1,4], R. E. Anthony[1,4], R. C. Aster[2], T. Taira[3], B. R. Shiro[4], D. C. Wilson[1,4], S. De Angelis[5], C. Ebeling[6], M. Haney[7], R. S. Matoza[8], and H. D. Ortiz[8]

[1]U.S. Geological Survey, Albuquerque Seismological Laboratory

[2]Colorado State University, Warner College of Natural Resources

[3]University of California, Berkeley

[4]U.S. Geological Survey, Geological Hazards Science Center

[5]University of Liverpool, Liverpool UK

[6]University of California, San Diego

[7]U.S. Geological Survey, Alaska Volcano Observatory

[8]Department of Earth Science and Earth Research Institute, University of California, Santa Barbara

April 2022

Summary

The eruption of the submarine Hunga Tonga-Hunga Ha‘apai (Hunga Tonga) volcano on January 15, 2022, was one of the largest volcanic explosions recorded by modern geophysical instrumentation. The eruption was notable for the broad range of atmospheric wave phenomena it generated and for their unusual coupling with the oceans and solid Earth. The event was

recorded worldwide across the Global Seismographic Network (GSN) by seismometers, microbarographs, and infrasound sensors. The broadband instrumentation in the GSN allows us to make high fidelity observations of spheroidal solid Earth normal modes from this event at frequencies near 3.7 and 4.4 mHz. Similar normal modes reported following the 1991 Pinatubo (Volcanic Explosivity Index of 6) eruption and were predicted, by theory, to arise from the excitation of mesosphere-scale acoustic modes of the atmosphere coupling with the solid Earth. Here, we compare observations for the Hunga Tonga and Pinatubo eruptions and find that both strongly excited the Earth normal mode ${}_0S_{29}$ (3.72 mHz) and that the modal amplitude was roughly 11 times larger for the 2022 Hunga Tonga eruption. Estimates of attenuation (Q) for ${}_0S_{29}$ across the GSN from temporal modal decay give Q=332±101, which is higher than estimates of Q for this mode using earthquake data (Q=186.9±5; Dziewonski and Anderson, 1981). Two microbarographs located at regional distances (< 1000 km) to the volcano provide direct observations of the fundamental acoustic mode of the atmosphere. These pressure oscillations, first observed approximately 40 minutes after the onset of the eruption, are in phase with the seismic Rayleigh wave excitation and are recorded only by microbarographs in proximity (< 1500 km) to the eruption. We infer that excitation of fundamental atmospheric modes occurs within a limited area close to the site of the eruption, where they excite select solid Earth fundamental spheroidal modes of similar frequencies that are globally recorded and have a higher apparent Q due to the extended duration of atmospheric oscillations.

Keywords: Volcano seismology, surface waves and free oscillations, seismic instruments, acoustic properties

Introduction

The Hunga Tonga-Hunga Ha‘apai (Hunga Tonga) volcanic eruption began its most energetic phase at around 04:14:00 January 15, 2022, UTC and was rapidly identified as a seismic event and assigned a surface wave magnitude (M_s; 20 s period) of 5.8 (Bormann, 2012) by the U.S. Geological Survey National Earthquake Information Center (NEIC). However, earthquake magnitudes are not appropriate for scaling volcanic eruptions, and longer-period observations recorded by high signal-to-noise very broadband (VBB) seismographic networks (e.g., Ringler et al., 2022) can be used to rapidly parameterize volcanic source parameters. For example, using 10 to 1000 s period seismic observations across the Global Seismographic (GSN), GEOFOrschungsNetz (GEOFON), and GEOSCOPE Networks, Poli and Shapiro (2022) estimate the Hunga Tonga eruption to have a Volcano Explosivity Index (VEI) of 6, where the VEI is a semi-quantitative scale used to characterize the explosivity of eruptions (Newhall and Self, 1982). The VEI scale is based on estimates of the total volume of erupted products and the maximum height reached by the eruptive plume; as such VEI estimates are challenging for eruptions with complex source mechanisms including magma-water interaction, like Hunga Tonga (Matoza et al., 2014, Witze, 2022). Nonetheless, a VEI 6 places the Hunga Tonga eruption as the largest explosive eruption worldwide since the (significantly more temporally extended and magmatically voluminous) VEI 6 Pinatubo (Philippines) eruption of June 15, 1991 (NASA, 2022).

The 1991 eruption of Pinatubo occurred shortly after the development of modern VBB force-feedback seismometers and digital systems capable of recording long-period oscillations with high fidelity (Ringler et al., 2022). The GSN and other such networks were in the process of

being built out at this time. However, unique long-period spheroidal normal mode oscillations of the Earth were soon identified on the GSN station MAJO (Matsushiro, Japan) and at globally distributed International Deployment of Accelerometer (IDA) gravimeters (Kanamori and Mori, 1992; Widmer and Zürn, 1992). Unlike the multiple normal mode oscillations of the Earth generated by great earthquakes (e.g., Nishada, 2013; Schneider and Deuss, 2021), Pinatubo excited only two modal frequencies: a dominant oscillation at 4.44 mHz (225 s period), and a smaller amplitude oscillation at 3.68 mHz (272 s), producing a "bi-chromatic" spectrum. Using particle motions and estimates of propagation velocities, these signals were shown to be consistent with a Rayleigh wavefield (elliptical motion in the direction of wave propagation) originating from the Pinatubo region (Kanamori and Mori, 1992; Widmer and Zürn, 1992).

The excitation of such low frequency, bi-chromatic Rayleigh waves and their associated normal modes is rare. Zürn and Widmer (1996) searched for similar signals following eleven other significant volcanic eruptions, but were able to identify similar signals for the April 4, 1982, El Chichón (Mexico) eruption. In this case, a lower frequency spectral peak was observed at 3.70 mHz (270 s), along with the dominant peak was observed at 5.14 mHz (195 s). The uniqueness of a source process that excites just two distinct global Rayleigh waves with normal mode frequencies and the consistency of the lower frequency peak near 3.70 mHz led to the hypothesis that the signal resulted from coupling of eruption-excited atmospheric oscillations with the solid Earth (Kanamori and Mori, 1992; Widmer and Zürn, 1992). To the best of our knowledge, prior to our study, observations of these spectral peaks in microbarograph records have only been reported following the 1982 El Chichón eruption at Piñon Flats (California) and College Magnetic Observatory (Alaska), both over 1000 km from the volcano (Widmer and Zürn, 1992).

Given the paucity of high signal-to-noise observations, current understanding of atmospheric modal excitation and its coupling with the solid Earth is principally informed by theory. Several studies have noted that characteristic temperature profiles in the atmosphere predict a fundamental acoustic-gravity mode near 3.68 mHz (Jones and Georges, 1976; Tahira, 1995; Lognonné et al., 1998; Dahlen and Tromp, 1998; Watada and Kanamori, 2010), which corresponds to the lower frequency peak excited by the Pinatubo and El Chichón eruptions. Taihira (1995) modeled this oscillation as an acoustic-gravity standing wave at frequencies of 3.64 to 3.69 mHz with an evanescent upper boundary and a wavelength λ of approximately four times the height of the mesopause (λ = 380 to 400 km). Similarly, the first atmospheric harmonic of this mode occurs at 4.40 mHz, but modeling suggests it should attenuate much more rapidly than the fundamental mode due to energy leakage from the upper mesophere (Lognonné et al., 1998) as well as its lower intrinsic quality factor Q. Lognonné et al. (1998) estimates Q to be 117 for the 3.68 mHz mode and 21 for the 4.40 mHz mode (Dahlen and Tromp, 1998; Table 8.3). Therefore, it is unclear why this frequency was the dominant excitation for the 1991 Pinatubo eruption or why it was absent for the 1982 El Chichón eruption. Similarly, open questions remain regarding the distance at which these atmospheric modes can be directly observed in microbarograph records (Kanamori et al., 1994).

In this study, we leverage instrumentation improvements across the modern GSN to document global observations of the excitation of 3.72 mHz Rayleigh waves following the 2022 Hunga Tonga eruption. We first perform spectral analysis on the event and identify the amplitude and frequency of spectral peaks excited by the event across the world. We then use these

observations of the Hunga Tonga eruption to determine Q for the spectral peak at 3.72 mHz. Next, we compare amplitudes of spectral peaks excited by the 1991 Pinatubo eruption to the 2022 Hunga Tonga eruption. Lastly, we examine microbarograph records across the GSN following the 2022 Hunga Tonga eruption to search for the excitation of predicted atmospheric normal modes (e.g., Tahira, 1995; Lognonné et al., 1998; Watada and Kanamori, 2010).

Global Observations of the Hunga Tonga Eruption

We examine all available long-period, high-gain, vertical component (channel LHZ; 1 sample/s) seismic data recorded on the primary sensors (location code 00) across the GSN for the 1991 Pinatubo and 2022 Hunga Tonga eruptions. We have restricted our attention to vertical component data as the signals of interest have a better signal-to-noise ratio (SNR) due to their lower sensitivity to tilt noise over the horizontal components (Beauduin et al., 1996). The GSN currently consists of 140 VBB high-dynamic-range seismic stations (Figure 1) capable of recording ground motions with frequency contents spanning diurnal Earth tides (0.0115 mHz) to high-frequency seismic signals up to many tens of Hz. In the last two decades, many GSN stations have been augmented with additional geophysical instrumentation, including microbarographs (Figure 1, blue). This makes it possible to examine the joint excitation of both the seismic and atmospheric modes for 2022 Hunga Tonga eruption. For this eruption, 112 of the 140 GSN stations recorded suitable vertical-component long-period seismic data for this analysis (e.g., no outages or significant data gaps).

The global excitation of the Earth from the Hunga Tonga eruption is readily observed in both microbarograph (Figure 2a) and seismic data (Figure 2b) with initial observations of these

arrivals reported in Matoza et al. (2022) and Yuen et al. (2022). To illustrate different phases, Figure 3 shows the vertical waveforms as recorded by GSN station ANMO (Albuquerque, New Mexico) for the microbarograph (Figure 3a) as well as the vertical component seismic (Figure 3b), which are located approximately 9500 km from Honga Tonga. In Figure 3 seismic data are filtered into bands of 10 to 40 mHz (green), 3 to 50 mHz (orange), and 3 to 5 mHz (red). P-waves and surface waves with dominant energy above 10 mHz are the first arrivals at GSN stations following the event (Figure 2a and 3b; Matoza et al., 2022). Body-wave arrivals are immediately followed by oscillations below 5 mHz that visually appear monochromatic and that "ring" for over 15 hours following the eruption (Figure 3b, red). The atmospheric Lamb acoustic-gravity wave from the eruption is clearly seen in GSN microbarograph data (Figure 2a) and travels at a global average velocity of 310 m/s (Matoza et al., 2022; blue line in Figure 2a), closely followed by infrasonic arrivals ($f > 0.01$ Hz). Many infrasound signals generated by explosions (e.g., Anthony et al., 2022; Edwards et al., 2007; Matoza et al., 2019) produce ground motions (Figure 3b, green) that are induced by these atmospheric perturbations (Figure 3a) through local pressure deformation of the solid Earth. However, for atmospheric signals with lower frequency content (< 3mHz) it is possible that Newtonian attraction can be the dominate signal (Zürn and Wielandt, 2007). The comparatively low velocity of the acoustic signals, one order of magnitude below the longer-period Rayleigh wave phase velocities of the Earth, implies that these pressure changes do not couple efficiently into an elastic surface wave (e.g., Kanamori and Mori, 1992; Watada and Kanamori, 2010).

Solid Earth Normal Modes

To characterize the extended lower frequency harmonic oscillation (i.e., normal modes), we process vertical-component seismic data to form spectral estimates between 3 to 6 mHz. We use 15-hour data segments (1.1Q cycles for Q=190; Dahlen, 1982) starting at 04:14:00 January 15, 2022 UTC for the Hunga Tonga eruption and 06:30:00 June 15, 1991 UTC for the Pinatubo eruption. For each data segment, we remove a least-squares linear trend, apply a Kaiser window taper with a β shape factor of 2π (Harris et al., 2020), and zero-pad the data to the next power of 2 (in this case 2^{16} samples). We then compute the discrete Fourier transform (DFT) and remove the instrument response in the appropriate band via spectral division. This yields a sample spacing of is 0.015 mHz in the frequency domain. An example of these spectra across the GSN for the Hunga Tonga eruption is shown in Figure 4. For reference we include the frequencies of spheroidal modes in the 3.6 mHz and 4.4 mHz regions calculated from Mineos (Masters et al., 2014) using the Preliminary Reference Earth Model (PREM; Dziewonski and Anderson, 1981). While different models of the Earth could produce different frequencies and quality factors (Montagner and Kennett, 1996), we only use eigenfrequencies computed by PREM as this is what is used in Lognonné et al. (1998). Beyond the model being used, not accounting for Coriolis coupling (Masters et al., 1983) or crustal corrections (Lekić et al., 2010) could produce differences between the estimated frequency and those observed, however we are only using the reference frequencies for mode identification and therefore did not apply these additional corrections. We have also included the frequencies of the atmospheric modes between the solid Earth modes ${}_0S_{28}$-${}_0S_{29}$ (3.68 mHz, orange) and ${}_0S_{36}$-${}_0S_{37}$ (4.40 mHz, green) from Lognonné et al. (1998). In describing the atmospheric modes, we use the notation of Dahlen and Tromp (1998;

Section 8.8.12), where ${}_0S_l$-${}_0S_{l'}$ indicates the atmospheric mode with a frequency lying between the solid Earth fundamental modes ${}_0S_l$ and ${}_0S_{l'}$, and l and l' are angular degree values.

Figure 4 shows obvious spectral peaks in the 3.5-3.8 mHz frequency band at nearly every GSN station; peaks near 4.4 mHz, however, are less clear. To quantify this excitation, we estimate the SNR of the excitation in the 3.5-3.8 mHz and 4.3-4.6 mHz bands using the peak amplitude within these bands as the signal and the peak amplitude in the 4.0-4.3 mHz and 5.0-5.3 mHz bands as the noise, respectively. Of the 112 stations considered, we find that 97 (blue, Figure 4) recorded oscillations near 3.7 mHz with a SNR greater than 3. In contrast, only 7 stations had a spectral peak with SNR greater than 3 near 4.4 mHz. Due to lack of high SNR observations, we do not consider the 4.4 mHz peak in subsequent peak frequency, amplitude, or attenuation analysis.

We plot the amplitude (Figure 5a) and corresponding peak frequency (Figure 5b) between 3.5 and 3.8 mHz across the GSN. Stations with SNR < 3 in this band are plotted as squares to indicate that we have less confidence in the measurements. Excluding these stations, we estimate this mode has a mean frequency of the excitation to be 3.72 mHz with a standard deviation of 0.0164 mHz (roughly the sample spacing in our spectra; 0.0152 mHz) by way of estimating the frequency of the peak. Notably, this frequency aligns closely with the solid Earth mode ${}_0S_{29}$ (3.72 mHz) as calculated from PREM (Dziewonski and Anderson, 1981). Stations PFO (Piñon Flat, California) and ADK (Aleutian Islands, Alaska) are notable outliers with peak frequencies of 3.63 mHz and 3.65 mHz, respectively (Figure 5b) which more closely align with the frequency of ${}_0S_{28}$ (3.63 mHz).

Amplitude measurements across the GSN are more variable than peak frequency observations (Figure 5a). The median spectral amplitude was 0.49 nm/s^2 with a standard deviation of 0.45 nm/s^2. Amplitudes at most (84%) stations are less than 0.6 nm/s^2, but we observe larger (> 1.0 nm/s^2) ground motions across many of the southwest Pacific islands, central Africa, and at the station PAB (San Pablo, Spain). We did not attempt to correct for any excitation pattern by way of stacking as the mode was excited at all stations (e.g., Dahlen and Tromp, 1998; Section 10.6). Following Masters et al. (1982) we include these values as a function of the antipode of the great circle through the station and the Honga Tonga eruption in Figure S1.

Estimate of Attenuation: We estimate Q of ${}_0S_{29}$ (3.72 mHz) following the eruption by measuring the decay of spectral estimates at stations across the GSN in the 3.65 mHz to 3.78 mHz band in subsequent time windows following the methodology of Sailor and Dziewonski (1978). We use this method as it does not require information about the source-time-function (which at the time of this writing was unavailable), which would be required to produce synthetics used to estimate attenuation (e.g., Talavera-Soza and Deuss, 2020). We consider a 30-hour record of data following the eruption and calculate spectra in 15-hour windows that move through the record in 1-hour steps (Figure S2). In total, we calculate 16 spectra for each GSN station. We then estimate the average power (P_{avg}) from each spectrum in our record using a trapezoid rule integration approach (Sailor and Dziewonski, 1978). After estimating the average power we estimate the slope m of $ln(P_{avg})$ from each time window as a function of time. This slope provides an estimate of Q=-2p/mf_{avg}, where f_{avg} is taken to be the average frequency in the band. To quantify how well the decay of the mode is modeled by the linear regression, we also

estimate the goodness of fit by estimating the residual between the data and linear regression in the least squares sense as decay of the natural logarithm of the average power should be approximately linear.

Estimates of Q for individual stations for the Honga Tonga eruption's excitation of ${}_0S_{29}$ are plotted in Figure S3. We consider stations with a residual less than 1 to be consistent with the exponential decay of ${}_0S_{29}$ and plot these stations as circles. In supplemental Figure S4 we include the Q estimates as a function of the antipodes of a great-circle between the station and the Hunga Tonga eruption (Maters et al., 1982). If we consider only stations with a residual below 1, we estimate a mean Q of 332 with a standard deviation of 101, which is significantly greater than the 186.9 (with a standard deviation of 5) predicted by PREM (Dziewonski and Anderson, 1981). Our attenuation measurement has relatively high scatter across the GSN stations and we do not observe clear spatial (Figure S3) or great circle (Figure S4) trends indicative of sensitivity to mantle structure. The method of Sailor and Dziewonski (1978) is weakly dependent on window size; however, we consistently obtain higher Q values than predicted by PREM even when adjusting the window between 10 and 20 hours.

Comparison to 1991 Pinatubo Eruption: Although the GSN was still in its infancy in 1991, 17 stations that recorded the 2022 Honga Tonga event also recorded the Pinatubo eruption (Figure 6). To eliminate any stations that did not record solid Earth modes excited by either eruption with low SNR, we removed all spectra with a peak amplitude greater than 0.6 nm/s^2 in the 3.9 to 4.1 mHz band and greater than 0.35 nm/s^2 in the 3.0 to 3.4 mHz band, as these spectra were dominated by noise. To show differences in the frequencies that were excited between the

Pinatubo and Hunga Tonga eruptions, we scale the Hunga Tonga spectra (Figure 6, blue) at each station so that the amplitude of the peak spectra between 3 and 6 mHz is identical to the Pinatubo spectra (Figure 6, brown). The scale factors applied to the Hunga Tonga spectra are shown in the right side of the figure.

We find that when stacking all available GSN stations (Figure 7), both the 1991 Pinatubo eruption (orange; 16 stations in stack) and the 2022 Hunga Tonga eruption (green; 112 stations in stack) predominantly excited the solid Earth fundamental mode $_0S_{29}$ (3.72 mHz). However, we find that the excitation of $_0S_{29}$ was more than 11 times larger for the Hunga Tonga eruption when all stations that recorded the event are included. When considering the 17 individual stations that recorded both events (Figure 6), 10 recorded peak amplitudes that were more than 5 times larger for the Hunga Tonga event.

The 2022 Hunga Tonga eruption excited additional fundamental modes of the Earth (as calculated from PREM; Dziewonski and Anderson, 1981) that are not visible in the Pinatubo eruption GSN stack (Figure 7) including $_0S_{28}$ (3.63mHz), $_0S_{30}$ (3.81 mHz), $_0S_{38}$ (4.53 mHz), and $_0S_{39}$ (4.62 mHz). We note that although we do not observe any peaks near 4.44 mHz (e.g., Widmer and Zürn, 1992) for the Pinatubo eruption when stacking the 16 stations, peaks around this frequency are clearly observed at individual stations (Figure 6).

Atmospheric Modes

We processed the atmospheric pressure data (location code LDO or LDI) at all 89 GSN stations that had microbarographs using the same procedure as the seismic data, described above (Figure

4) except we use a 26-hr time series to account for the slower velocity of the atmospheric waves. Although this is longer than the 1.1Q-cycle time window (Dahlen 1982), this is necessary because it takes the Lamb acoustic-gravity wave nearly 18 hours after the eruption to reach the antipode (e.g., Figure 2a). All pressure data used were recorded by well calibrated pressure transducers (location codes 31 or 00). Although all operating microbarographs recorded the initial Lamb wave and infrasound signals produced by the eruption, the only stations where the SNR of the microbarograph was above 3 in the 3.5 to 3.8 mHz band were MSVF (Monasavu, Fiji) and OBN (Obninsk, Russia). Data from station OBN were dominated by noise and produced a false positive, as visual inspection doesn't show a distinct peak in the 3.5 to 3.8 mHz region. Station AFI (Afiamalu, Samoa) potentially recorded the excitation of a peak in the 3.5 to 3.8 mHz band, but it had relatively poor SNR (Figure S5) and the lack of excitation could have also come from source directivity (Kim et al., 2012). We did observe an even lower frequency signal (approximately 2.78 mHz) at station AFI that was also observed on an AGBOM microbarograph in Samoa (Figure S5). We do note that no microbarographs recorded a spectral peak with an SNR greater than 3 in the 4.3 to 4.6 mHz region (Figure S6).

Pressure oscillations around 3.7 mHz at MSVF do not appear until about 40 minutes following the eruption and occur in several episodic pulses roughly coincident with seismic energy (Figures 8 and 9). The first pulses following the eruption show pressure oscillations that are in phase with of seismic accelerations, but this does not hold true for later arrivals. Applying a least-squares pressure correction, similar to the method described in Zürn and Widmer (1995) and further discussed in Zürn and Meurers (2009), we found only a 33% reduction in variance (Figure 8, green). Our estimated correction coefficient was 13.3 nm/s^2/hPa. This value is much

larger than any of those estimated by Zürn and Meurers (2009) in their Table 1 and opposite in sign. Their values are all near 4 nm/s^2/hPa. The pressure and seismic records at MSVF provide a local example near the notch frequency discussed in Zürn and Wielandt (2007). We note here again that seismic energy bandpass filtered around ${}_0S_{29}$ decays more slowly than would be predicted by PREM (Figure 9c).

Discussion

We suggest that these pressure oscillations at 3.71 and 3.73 mHz recorded on MSVF represent the first direct observation of excitation of the fundamental mode of the atmosphere since microbarograph observations at Piñon Flats (California) following the 1982 El Chichón eruption (Widmer and Zürn, 1992). Coupling of this atmospheric mode into the solid Earth was modeled by several studies to explain the seismic observation following the 1991 Pinatubo eruption (Tahira, 1995; Lognonne, 1998; Watada and Kanamori, 2010). However, nearby direct pressure observations during the eruption lacked sufficient timing accuracy to enable a direct observation of this mode (Widmer and Zürn, 1992). Other studies have observed nearfield atmospheric oscillations at different frequencies (e.g., Kanamori et al., 1994), but the interpretations and robustness have been questioned (Watada and Kanamori, 2010). For the Hunga Tonga eruption, our observation of the microbarograph oscillation at ~3.7 mHz is in phase with the vertical seismic acceleration at MSVF (Figure 8). As we discuss below, we observe a similar atmospheric excitation from a second, regional (~68 km) microbarograph located in Tonga and demonstrate that the observed attenuation of 3.7 mHz pressure variations at this station is consistent with theoretical modeling of the fundamental mode of Earth's atmosphere. Therefore, our observations following the 2022 Hunga Tonga eruption support these previous models that

global excitation of ${}_0S_{29}$ following large volcanic eruptions results from local excitation of the fundamental mode of the atmosphere and subsequent coupling into the solid Earth.

We estimate the Q of ${}_0S_{29}$ across the GSN following the 2022 Hunga Tonga eruption and find Q=332±101 which is much larger than the Q=186.9 for mode ${}_0S_{29}$ predicted by PREM. We interpret the higher measured values of Q as resulting from an extended eruption duration coupled with the relatively slow decay of the induced atmospheric pressure oscillations. For instance, Poli and Shapiro (2022) estimate the eruption duration to be more than 6000 s, which is about 40 times longer than the rupture duration of the M_w 9.0 2011 Tohoku earthquake (Ammon et al., 2011). Logonné et al. (1998) estimate Q of the fundamental atmospheric mode to be 114.7. Therefore, even an impulsive excitation of this atmospheric mode will generate pressure oscillations at Earth's surface for several hours and Rayleigh waves (excited from these pressure oscillations) will continue to be generated near the volcanic source even after the eruption has ceased. We also estimated elevated Q values for the Pinatubo event (Q=399±93), which we note agrees with the Hunga Tonga estimate and is also substantially higher than predicted by PREM (Figure S7). However, since only a few stations were available, our confidence in these estimates is less than for the Hunga Tonga event.

We directly record this extended atmospheric source duration in the raw pressure data at MSVF, where oscillations around 3.7 mHz are recorded for several hours following the eruption (Figure 9b). Although not a GSN station, we did observe similar 3.7 mHz pressure oscillations on a barometer located in Tonga from the Australian Government Bureau of Meteorology (AGBOM, Figure 10) roughly 68 km from the eruption. Here, the peak frequency of excitation is 3.73 mHz

(with a subpeak at 3.70 mHz) and peak pressure exceeding 100 Pa and can be visually observed in raw pressure data for at least 9 hours following the eruption. We estimate Q of the fundamental mode of the atmosphere using pressure records in Tonga similarly to how we estimated Q of ${}_0S_{29}$ from seismic records. Because the signal decays faster, we instead consider only 12 hours and step through the data in half hour increments with 6-hour spectral windows. Using this technique, we arrive at a Q estimate of the atmosphere of 111.8, which is quite close to the modeled quality factor of Q=114.7 (Logonné et al., 1998; Figure 11a).

Although the fundamental mode of the atmosphere is observed in pressure data at MSVF (755 km from the volcano), this mode is not observed at publicly available pressure sensors across the globe including at the GSN station RAR (Raratonga; approximately 1500 km from the volcano). While we potentially also observed this signal at AFI (Afiamalu, Samoa; approximately 831 km from the volcano), the SNR of the mode at that station was too low for us to definitively declare a detection there (Figure S5). It is possible that the spatial area of atmospheric to ground coupling may be limited to a radius of less than 1000 km from the volcano. Notably, this is significantly larger than the 37 km radius modeled for the first atmospheric harmonic (~4.4 mHz) following the 1991 Pinatubo eruption (Kanamori and Mori, 1992).

However, the long source-time function of the eruption could complicate our ability to understand the region of atmospheric to ground coupling. It is also possible that we are not able to resolve some pressure oscillations at more distant and azimuthally distributed sensors due to attenuation and higher background noise levels from wind or pressure source directivity (e.g., Kim et al., 2012). To our knowledge, the only previous observation of the fundamental

atmospheric mode following an eruption was from the 1982 El Chichón eruption at PFO (Piñon Flats, California) at approximately 3000 km from the volcano (Widmer and Zurn, 1992). Therefore, questions remain regarding the spatial extent to which the atmospheric excitation occurred.

We note that although we measure the peak frequency of the fundamental mode of the atmosphere at MSVF and in Tonga following the eruption of Hunga Tonga to between 3.71 and 3.73 mHz, the eigenfrequency of the mode is dependent on atmospheric structure and has been modeled to occur anywhere between 3.64 and 3.75 mHz depending on season and latitude (Tahira, 1995; Watada and Kanamori, 2010). A double-peak at 3.71 and 3.73 mHz is clearly observed in the spectra at MSVF, but this pattern is less clear on the Tonga microbarograph (Figure 11). It is unclear what is causing the double-frequency peak of the fundamental atmospheric mode at MSVF. The robustness of this observation is also questionable given the relatively limited 12-hour data window, but is a curious feature in this dataset.

Although the fundamental mode of the atmosphere can vary slightly (~0.1 mHz; Tahira, 1995) based on atmospheric structure, we observe consistent excitation of the spheroidal solid Earth fundamental mode ${}_0S_{29}$ (3.72 mHz) for both the 2022 Hunga Tonga eruption and the 1991 Pinatubo eruption (Figure 6). We note that the eigenfrequency we calculate for Pinatubo is slightly different than the 3.68 mHz (standard deviation of 0.02 mHz) reported by Widmer and Zürn (1992). This could be because Widmer and Zürn calculate spectra using 3-hr windows of data (Table 1 of Widmer and Zürn, 1992), which is in contrast to our 12-hr windows of data. Although Widmer and Zürn (1992) made their measurements on gravimeters and this study

mostly uses force-feedback seismometers (e.g., Streckeisen STS-1s), it is unlikely that this could produce a difference in the measured eigenfrequency.

We observe that the amplitude of ${}_0S_{29}$ excited by the 2022 Hunga Tonga eruption was over an order of magnitude larger than the same excitation from the 1991 Pinatubo eruption. The reason for this observation is unclear but could be related to how effectively each eruption excited the atmosphere and enabled solid Earth coupling, the area over which atmospheric-to-solid Earth coupling occurred, or potentially other differences in the source mechanisms between the two eruptions. This comparison is further complicated by the Pinatubo event being a subaerial volcano on land while the Hunga Tonga eruption was partially submerged (Pallister et al., 1992). The excitation of these low-frequency modes from the submerged nature of the Hunga Tonga eruption could be further complicated by taking place in a seawater environment (Thiéry and Mercury, 2009).

We hypothesize that more efficient coupling between the atmosphere and the solid Earth may occur when the atmospheric eigenfrequency is closer to a fundamental solid Earth mode and this could potentially have contributed to the higher amplitude excitations of ${}_0S_{29}$ following the Hunga Tonga eruption. Using a model of the atmosphere during the 1991 Pinatubo eruption, Watada and Kanamori (2010) estimate the eigenfrequency of the atmospheric fundamental mode as 3.68 mHz. Although there are no direct observations of the eigenfrequency of the atmosphere during the Pinatubo eruption, this suggests that 3.71 to 3.73 mHz atmospheric resonance of the 2022 Hunga Tonga eruption (Figure 11) may have been closer to the eigenfrequency of ${}_0S_{29}$ (3.72 mHz).

We also hypothesized that the extreme height of the eruption plume (≈55−58 km; NASA, 2022; Carr et al., 2022) generated by the Hunga Tonga eruption may have also played a role by more strongly exciting the fundamental mode of the atmosphere compared to the 1991 Pinatubo eruption (plume height ≈35 km; NASA, 2022) . Watada and Kanamori (2010) model that up to 50 km, excitation of both the fundamental mode (~3.7 mHz) and first harmonic (~4.4 mHz) of Earth's atmosphere becomes more efficient as the source altitude increases. Pressure oscillations (of unknown frequency content) following the 1991 Pinatubo eruption were observed 21 km from the volcano to have an amplitude of roughly 300 Pa (Kanamori and Mori, 1992). In contrast, pressure oscillations between 2.5 and 5 mHz following the Hunga Tonga eruption are roughly 200 Pa at AGBOM (Figure 10a) and 100 Pa MSVF (Figure 9b). Therefore, these observations suggest that atmospheric pressure oscillations generated by the Tonga eruption may not have been appreciably larger than those generated by Pinatubo.

Although previous studies note that the dominant excitation of the 1991 Pinatubo event is near 4.44 mHz (e.g., Kanamori et al., 1992; Widmer and Zürn, 1992), we observe that the eigenfrequency of this peak is highly variable across different GSN stations (Figures 6 and 7). In contrast, the Hunga Tonga eruption appears to have excited several fundamental modes of the Earth in the 3.7 mHz region as well as the 4.4 mHz region. The signals we observe are still largely "bi-chromatic," as described in Widmer and Zürn (1992), but we can see that several frequencies are excited in both regions including frequencies that correspond to ${}_0S_{28}$, ${}_0S_{29}$, ${}_0S_{30}$, ${}_0S_{37}$, ${}_0S_{38}$, and ${}_0S_{39}$ (Figure 7). We note that this excitation of several solid Earth modes outside of the fundamental mode and first harmonic of the atmosphere is not anticipated from recent

modeling (Watada and Kanamori, 2010). This could be a result of variations in the atmosphere near the eruption (e.g., pressure and temperature) as well as source processes as the eruption occurred under water. We do not see any obvious change in the frequencies being excited based on the distance to the event or the antipode (Figures 5b and S1). These excitations may result from variations in the atmosphere which would produce different frequencies (Lognonné et al., 1998). While the excitation of these modes is interesting, modeling their generation using more realistic Earth models (e.g., Bishop et al., 2021) could help to better understand these excitations and how the model can directly influence the excitation frequency.

Conclusions

The January 15, 2022 Hunga Tonga eruption provided the best opportunity since the 1991 Pinatubo eruption to record solid Earth normal modes generated through acoustic coupling of atmospheric normal modes. Similar to the 1991 Pinatubo eruption (and unlike earthquakes), when stacking ground motion spectra following the eruption we find unique "bi-chromatic" excitation of solid Earth modes near the frequencies of 3.7 and 4.4 mHz. Because these frequencies correspond to the fundamental and first harmonic frequencies of Earth's atmosphere, several models had been put forth following the Pinatubo eruption that the excitation of these discrete normal modes arose through acoustic coupling between the atmosphere and the solid Earth. Utilizing global seismic records as well as microbarograph records in proximity (<1000 km) to the eruption, we make several fundamental observations which largely support this modeling.

First, for the 2022 Hunga Tonga eruption, we measure the global quality factor, Q, of solid Earth normal mode ${}_0S_{29}$ to be 332±101, which is significantly higher than predicted by the PREM model (Q=186.9±5). This higher Q value is consistent with the extended seismic source duration presented in atmospheric-solid Earth coupling models. Second, we present pressure data recorded in proximity (<1000 km) to the eruption which display pronounced spectral peaks near 3.7 mHz. These measurements likely represent the highest fidelity recordings to date documenting excitation of the fundamental mode of Earth's atmosphere. At the closest micobarograph to the eruption (~68 km), pressure oscillation at 3.7 mHz exceed 200 Pa and we directly measure Q of these oscillation to be 111.8, which is close to what is predicted by theoretical modeling. At MSVF (Monasavu, Fiji), co-located seismic and pressure observations indicate that initial pressure and ground acceleration oscillations occur in phase. Taken together, these observations are consistent with the hypothesis that global observations of ${}_0S_{29}$ following the 1991 Pinatubo eruption resulted from excitation of a fundamental mode of the atmosphere, which subsequently coupled into the solid Earth. We show that only microbarographs in relatively close (<1000 km) proximity observe these pressure oscillations and suggest that this coupling may occur over a limited spatial scale. This explains why observations of Rayleigh waves following the eruption have travel times consistent with a source at the site of the eruption.

We also found many discrepancies between normal mode excitation following the two eruptions. Unlike the 1991 Pinatubo eruption, most individual seismic stations do not display spectral peaks in ground motion near 4.4 mHz and the overall dominant excitation (both in the atmosphere and solid Earth) occurred near 3.7 mHz. Although we found that the solid Earth mode ${}_0S_{29}$ (3.72

mHz) was excited by both eruptions, the excitation amplitude was roughly 11 times larger for the 2022 Hunga Tonga eruption than the 1991 Pinatubo eruption. The physical reason behind this observation is unclear, but it could be due to differences in source processes changing how the atmosphere was excited or differences in the regional atmospheric structure. We make several observations following the 2022 Hunga Tonga eruption that are not consistent with previous models (e.g., Lognonné et al., 1998), including the two spectral peaks in the pressure record at MSVF and the excitation of a suite of fundamental solid Earth modes following the eruption. This could be related to previous models using only one-dimensional radial Earth parameterizations, perhaps extending the methods of Bishop et al. (2021) to a global three-dimensional Earth model would partially resolve this issue.

The 2022 Hunga Tonga eruption is one of just three volcanic eruptions recorded with geophysical instrumentation suitable for detecting atmospherically coupled Solid Earth modes. We are confident that these observations will help to better constrain modeling of some of the less understood processes associated with modal coupling between the atmosphere and solid Earth.

Data and Resources

Most data used in this study were obtained through the facilities of the Incorporated Research Institutions for Seismology (IRIS)/U.S. Geological Survey (USGS) network (network code IU; ASL/USGS, 1988), the New China Digital Seismograph Network (network code IC; ASL/USGS, 1992), the Caribbean USGS Network (network code CU; ASL/USGS, 2006), as well as the International Deployment of Accelerometers (IDA) network (network code II;

Scripps Institution of Oceanography, 1986). These data are freely available at the IRIS Data Management Center (DMC).

The Tonga barometer data used in Figure 11 are available within the repository associated with this work (https://github.com/aringler-usgs/tonga_paper); that station is part of an Australian Aid project called Climate and Oceans Support Program in the Pacific (COSPPac) with stations across 13 Pacific Island countries. The maintenance, operations, and products of the tide and global navigation satellite systems (GNSS) stations within COSPPac are managed by Robert Greenwood (Australian Bureau of Meteorology) through the Pacific Sea Level and Geodetic Monitoring (PSLGM) project (http://www.bom.gov.au/pacific/projects/pslm/).

We relied heavily on the Python library ObsPy (Megies et al., 2011) as well as Cartopy (Met Office, 2015).

The facilities of IRIS Data Services, and specifically the IRIS DMC, were used for access to waveforms, related metadata, derived products used in this study. IRIS Data Services are funded through the Seismological Facilities for the Advancement of Geoscience and EarthScope (SAGE) Proposal of the National Science Foundation (NSF) under Cooperative Agreement EAR-1261681.

The Global Seismographic Network (GSN) is a cooperative scientific facility operated jointly by the IRIS, the USGS, and NSF, under Cooperative Agreement EAR-1261681.

R.S.M and H.D.O acknowledge NSF grant EAR-1847736.

S.D.A. acknowledges support from Royal Society International Exchange grant IES\R2\202007.

Any use of trade, firm, or product names is for descriptive purposes only and does not imply endorsement by the U.S. Government.

Author Contributions

A. T. Ringler: Conceptualization, Data curation, Formal analysis, Methodology, and Writing

R. E. Anthony: Conceptualization, Data curation, Formal analysis, Methodology, and Writing

R. C. Aster: Methodology and Writing

T. Taira: Conceptualization, Methodology, and Formal analysis

B. R. Shiro: Writing

D. C. Wilson: Writing

M. Haney: Data curation, Writing

S. De Angelis: Formal analysis, Writing

C. Ebeling: Writing

R. S. Matoza: Methodology and Writing

H. D. Ortiz: Methodology and Writing

Acknowledgements: This work has benefited from discussions along with a helpful review of the manuscript by Charles Hutt. We thank an anonymous reviewer, Rex Baum, Ryan Gold, Barbara Ralston, Simon Schneider, Liam Toney, and Rudolf Widmer-Schnidrig for careful reviews that

improved the manuscript. We thank Toshiro Tanimoto for suggesting an amplitude comparison with synthetic seismograms which led us to investigate several other pieces. This work benefited greatly from discussions with coauthors involved in the preparation of Matoza et al. (2022).

References

Albuquerque Seismological Laboratory (ASL)/U.S. Geological Survey (USGS) (1988). Global Seismograph Network (GSN–IRIS/USGS), *International Federation of Digital Seismograph Networks*, DOI: 10.7914/SN/IU.

Albuquerque Seismological Laboratory (ASL)/USGS (1992). New China digital seismograph network, *International Federation of Digital Seismograph Networks*, DOI: 10.7914/SN/IC.

Albuquerque Seismological Laboratory (ASL)/USGS (2006). Caribbean USGS Network, *International Federation of Digital Seismograph Networks*, DOI: 10.7914/SN/CU.

Ammon, C. J., T. Lay, H. Kanamori, and M. Cleveland (2011). A rupture model of the 2011 off the Pacific coast of Tohoku Earthquake, *Earth, Planets and Space*, **63**, 7, 33, 692-696, DOI:10.5047/eps.2011.05.015.

Anthony. R. E., J. Watzak, A. T. Ringler, and D. C. Wilson (2022). The nature and precision of direct acoustic-to-seismic coupling from local explosions, *Geophysical Journal International*, in press, DOI: 10.1093/gji/ggac154.

Beauduin, R., P. Lognonné, J.—P. Montagner, S. Cacho, J. F. Karczewski, and M. Morand (1996). The effects of atmospheric pressure changes on seismic signals or how to improve the quality of a station, *Bulletin of the Seismological Society of America*, **86**, 6, 1760-1769, DOI: 10.1758/BSSA0860061760.

Bishop, J. W., D. Fee, R. Modrak, C. Tape, and K. Kim (2021). Spectral element modeling of acoustic to seismic coupling over topography, *Journal of Geophysical Research: Solid Earth*, **127**, 1, e2021JB023142, DOI: 10.1029/2021JB023142.

Bormann, P. (2012). *New Manual of Seismological Observatory Practice* (NMSOP-2), *IASPEI*, *GFZ German Research Centre for Geosciences*, Potsdam, DOI: 10.2312/GFZ.NMSOP-2.

Carr, J. L., A. Horáth, D. L. Wu, and M. D. Friberg (2022). Stereo plume height and motion retrievals for the record-setting Hunga Tonga-Hunga Ha'apai Eruption of 15 January, 2022, in review with *Geophysical Research Letters*, **49**, e2022GL098131, DOI: 10.1029/2022GL098131.

Dahlen, F. A. (1982). The effect of data windows on the estimation of free oscillation parameters, *Geophysical Journal International*, **69**, 2, 537-549, DOI: 10.1111/j.1365-246X.1982.tb04964.x.

Dahlen, F. A., and J. Tromp, (1998). Theoretical Global Seismology, Princeton University Press, Princeton, New Jersey, 1025 pp.

Dziewonski, A. M., and D. L. Anderson (1981). Preliminary reference Earth model, *Physics of the Earth and Planetary Interiors*, **25**, 4, 297-356, DOI: 10.1016/0031-9201(81)90046-7.

Edwards, W. N., D. W. Eaton, P. J. McCausland, D. O. ReVelle, and P. G. Brown (2007). Calibrating infrasonic to seismic coupling using the Stardust sample return capsule shockwave: Implications for seismic observations of meteors, *Journal of Geophysical Research*, **112**, B10, B10306, DOI: 10.1029/2006JB004621.

Harris, C. R., K. J. Millman, S. J. van der Walt, R. Gommers, P. Virtanen, D. Cournapeau, E. Wieser, J. Taylor, S. Berg, N. J. Smith, R. Kern, M. Picus, S. Hoyer, M. H. van Kerkwijk, M. Brett, A. Haldane, J. Fernández del Río, M. Wiebe, P. Peterson, P. Gérard-Marchant, K. Sheppard, T. Reddy, W. Weckesser, H. Abbasi, C. Gohlke, and T. E. Oliphant (2020). Array programming with NumPy, *Nature*, **585**, 357-362, DOI: 10.1038/s41586-020-2649-2.

Jones, R. M., and T. M. Georges (1976). Infrasound from convective storms. III. Propagation to the ionosphere, *The Journal of the Acoustical Society of America*, **59**, 4, 765-779, DOI: 10.1121/1.380942.

Kanamori, H. and J. Mori (1992). Harmonic excitation of the mantle Rayleigh waves by the 1991 eruption of Mount Pinatubo, Philippines, *Geophysical Research Letters*, **19**, 7, 721-724, DOI: 10.1029/92GL00258.

Kanamori, H., J. Mori, and D. G. Harkrider (1994). Excitation of atmospheric oscillations by volcanic eruptions, *Journal of Geophysical Research*, **99**, B11, 21947-21961, DOI: 10.1029/94JB01475.

Kim, K. J. M. Lees, and M. Ruiz (2012). Acoustic multipole source model for volcanic explosions and inversions for source parameters, *Geophysical Journal International*, **191**, 3, 1192-1204, DOI: 10.1111/j.1365-246X.2012.05696.x.

Lekić, V., M. Panning, and B. Romanowicz (2010). A simple method for improving crustal corrections in waveform tomography, *Geophysical Journal International*, **182**, 1, 265-278, DOI: 10.1111/j.1365-246X.2010.04602.x.

Lognonné, P., and E. Clévédé, and H. Kanamori (1998). Computation of seismograms and atmospheric oscillations by normal-model summation for a spherical earth model with realistic atmosphere, *Geophysical Journal International*, **135**, 2, 388-406, DOI: 10.1046/j.1365-246X.1998.00665.x.

Masters, G., M. Barmine, and S. Kientz (2014). Mineos user manual version 1.0.2, 99 pp., Available at: https://geodynamics.org/cig/software/mineos/mineos-manual.pdf, last accessed: February 2022.

Masters, G., J. Park, and F. Filbert (1983). Observations of coupled spheroidal and toroidal modes, *Journal of Geophysical Research: Solid Earth*, **88**, B12, 10,285-10,298, DOI: 10.1029/JB088iB12p10285.

Masters, G., T. H. Jordan, P. G. Silver, and F. Gilbert (1982). Aspherical Earth structure from fundamental spheroidal-mode data, *Nature*, **298**, 609-613, DOI: 10.1038/298609a0.

Matoza, R. S., A. Arciniega-Ceballos, R. W. Sanderson, G. Mendo-Pérez, A. Rosado-Fuentes, and B. A. Chouet (2019). High-broadband seismoacoustic signature of Vulcanian explosions at Popocatépetl volcano, Mexico, *Geophysical Research Letters*, **46**, 1, 148-157, DOI: 10.1029/2018GL080802.

Matoza, R. S., D. Fee, and T. M. López (2014). Acoustic characterization of explosion complexity at Sakurajima, Karymsky, and Tungurahua volcanoes, *Seismological Research Letters*, **85**, 6,1187-1199, DOI: 10.1785/0220140110.

Matoza, R. S., D. Fee, J. D. Assink A. M. Iezzi, D. N. Green, K. Kim, L. Toney, T. Lecocq. S. Krishnamoorthy, J-. M. Lalande, K. Nishida, K. L. Gee, M. M. Haney, H. D. Ortiz, Q. Brissaud, L. Martire, L. Rolland, P. Vergados, A. Nippress, J. Park, S. Shani-Kadmiel, A. Witsil, S. Arrowsmith, C. Caudron, S. Watada, A. B. Perttu, B. Taisne, P. Mialle, A. Le Pichon, J. Vergoz, P. Hupe, P. S. Blom, R. Waxler, S. De Angelis, J. B. Snively, A. T. Ringler, R. E. Anthony, A. D. Jolly, G. Kilgour, G. Averbuch, M. Ripepe, M. Ichihara, A. Arciniega-Ceballos, E. Astafyeva, L. Ceranna, S. Cevuard, I-.Y. Che, R. De Negri, C. W. Ebeling, L. G. Evers, L. E. Franco-

Marin, T. B. Gabrielson, K. Hafner, R. Giles Harrison, A. Komjathy, G. Lacanna, J. Lyons, K. A. Macpherson, E. Marchetti, K. F. McKee, R. J. Mellors, G. Mendo-Pérez, T. D. Mikesell, E. Munaibari, M. Oyola-Merced, I. Park, C. Pilger, C. Ramos, M. C. Ruiz, R. Sabatini, H. F. Schwaiger, D. Tailpied, C. Talmadge, J. Vidot, J. Webster, D. C. Wilson (2022). Atmospheric waves and global seismoacoustic observations of the January 2022 Hunga eruption, Tonga, *Science*, DOI: 10.1126/science.abo7063.

Megies, T., M. Beyreuther, R. Barsch, L. Krischer, and J. Wassermann (2011). ObsPy – What can it do for data centers and observatories?, *Annals of Geophysics*, **54**, 47-58, DOI: 10.4401/ag-4838.

Met Office (2015). Cartopy: A cartographic Python library with a Matplotlib interface, Exter, Devon, https://scitools.org.uk/cartopy, DOI: 10.5281/zenodo.1182735.

Montagner, J. -P. and B. L. N. Kennett (1996). How to reconcile body-wave and normal mode reference Earth models, *Geophysical Journal International*, **125**, 1, 229-248, DOI: 10.1111/j.1365-246X.1996.tb06548.x.

NASA (2022). Tonga volcano plume reached the mesosphere, *NASA Earth Observatory*, https://earthobservatory.nasa.gov/images/149474/tonga-volcano-plume-reached-the-mesosphere, last accessed: March 2022.

Newhall, C. G. and S. Self (1982). The volcanic explosivity index (VEI) an estimate of explosive magnitude for historical volcanism, *Journal of Geophysical Research: Oceans*, **82**, C2, 1231-1238, DOI: 10.1029/JC087iC02p01231.

Nishida, K. (2013). Earth's background free oscillations, *Annual Review of Earth and Planetary Sciences*, **41**, 719-740, DOI: 10.1146/annurev-earth-050212-124020.

Nishida, K., N. Kobayashi, and Y. Fukao (2014). Background Lamb waves in the Earth's atmosphere, *Geophysical Journal International*, **196**, 1, 312-316, DOI: 10.1093/gji/ggt413.

Pallister, J. S., R. P. Hoblitt, and A. G. Reyes (1992). A basalt trigger for the 1991 eruptions of Pinatubo volcano?, *Nature*, **356**, 426-428, DOI: 10.1038/356426a0.

Peterson, J. (1993). Observations and Modeling of Seismic Background Noise, *U.S. Geological Survey Open-File Report*, **93-322**, 94 pp, DOI: 10.3133/ofr93322.

Poli, P., and N. M. Shapiro (2022). Rapid characterization of large volcanic eruptions: Measuring the impulse of the Hunga Tonga explosion from teleseismic waves, *in review*, DOI: 10.1002/essoar.10510358.1.

Ringler, A. T., R. E. Anthony, R. C. Aster, C. J. Ammon, S. Arrowsmith, H. Benz, C. Ebeling, W. -Y. Kim, P. Koelemeijer, H. C. P. Lau, V. Lekić, J. P. Montagner, P. G. Richards, D. P.

Schaff, M. Vallée, and W. Yeck (2022). Achievements and prospects of global broadband seismic networks after 30 years of continuous geophysical observations, *in review*.

Sailor, R. V. and A. M. Dziewonski (1978). Measurements and interpretation of normal mode attenuation, *Geophysical Journal International*, **53**, 3, 559-581, DOI: 10.1111/j.1365-246X.1978.tb03760.x.

Schneider, S., and A. Deuss (2021). A new catalogue of toroidal-mode overtone splitting function measurements, *Geophysical Journal International*, **225**, 1, 329-341, DOI: 10.1093/gji/ggaa567.

Tahira, M. (1995). Acoustic resonance of the atmosphere at 3.7 mHz, *Journal of Atmospheric Sciences*, **52**, 15, 2670-2674, DOI: 10.1175/1520-0469(1995)052<2670:AROTAA>2.0.CO;2.

Talavera-Soza, S., and A. Deuss (2020). New measurements of long-period radial modes using large earthquakes, *Geophysical Journal International*, **224**, 2, 1211-1224, DOI: 10.1093/gji/ggaa499.

Scripps Institution of Oceanography (1986). IRIS/IDA Seismic Network, *International Federation of Digital Seismograph Networks*, DOI: 10.7914/SN/II.

Thiéry, R. and L. Mercury (2009). Explosive properties of water in volcanic and hydrothermal systems, *Journal of Geophysical Research*, **114**, B5, B05205, DOI: 10.1029/2008JB005742.

Watada, S. and H. Kanamori (2010). Acoustic resonant oscillations between the atmosphere and the solid earth during the 1991 Mt. Pinatubo eruption, *Journal of Geophysical Research*, **115**, 12, B12319, DOI: 10.1029/2010JB007747.

Widmer, R. and W. Zürn (1992). Bichromatic excitation of long-period Rayleigh and air waves by the Mount Pinatubo and El Chichon volcanic eruptions, *Geophysical Research Letters*, **19**, 8, 765-768, DOI: 10.1029/92GL00685.

Witze, A. (2022). Why the Tongan eruption will go down in the history of volcanology, *Nature*, **602**, 376-378, DOI: 10.1038/d41586-022-00394-y.

Yuen, A. D., M. A. Scruggs, F. J. Spera, Y. Zheng, H. Hu, S. R. McNutt, G. Thompson, K. Mandli, B. R. Keller, S. Shawn Wei, Z. Peng, Z. Zhou, F. Mulargia, and Y. Tanioka (2022). Under the surface: Pressure-induced planetary-scale waves, volcanic lightning, and gaseous clouds caused by the submarine eruption of Hunga Tonga-Hunga Ha'apai volcano, *Earthquake Research Advances*, DOI: 10.1016/j.eqrea.2022.100134.

Zürn, W. and B. Meurers (2009). Clear evidence for the sign-reversal of the pressure admittance of gravity near 3 mHz, *Journal of Geodynamics*, **48**, 371-377, DOI: 10.1016/j/jog.2009.09.040.

Zürn, W. and R. Widmer (1995). On noise reduction in vertical seismic records below 2 mHz using local barometric pressure, *Geophysical Research Letters*, **22**, 24, 3537-3540, DOI 10.1029/95GL03369.

Zürn, W. and R. Widmer (1996). World wide observations of bichromatic long-period Rayleigh-waves excited during the June 15, 1991 eruption of Mt. Pinatubo, in *Fire and Mud, Eruptions of Mount Pinatubo, Phillipines*, pp. 615-624, eds Newhall, C. and J.R. Punongbayan, Phillipine Institute of Volcanology and Seismology, Quezo City and University of Washington Press.

Zürn W., and E. Wielandt (2007). On the minimum of vertical seismic noise near 3 mHz, *Geophysical Journal International*, **168**, 2, 647-658, DOI: 10.1111/j.1365-246X.2006.03189.x.

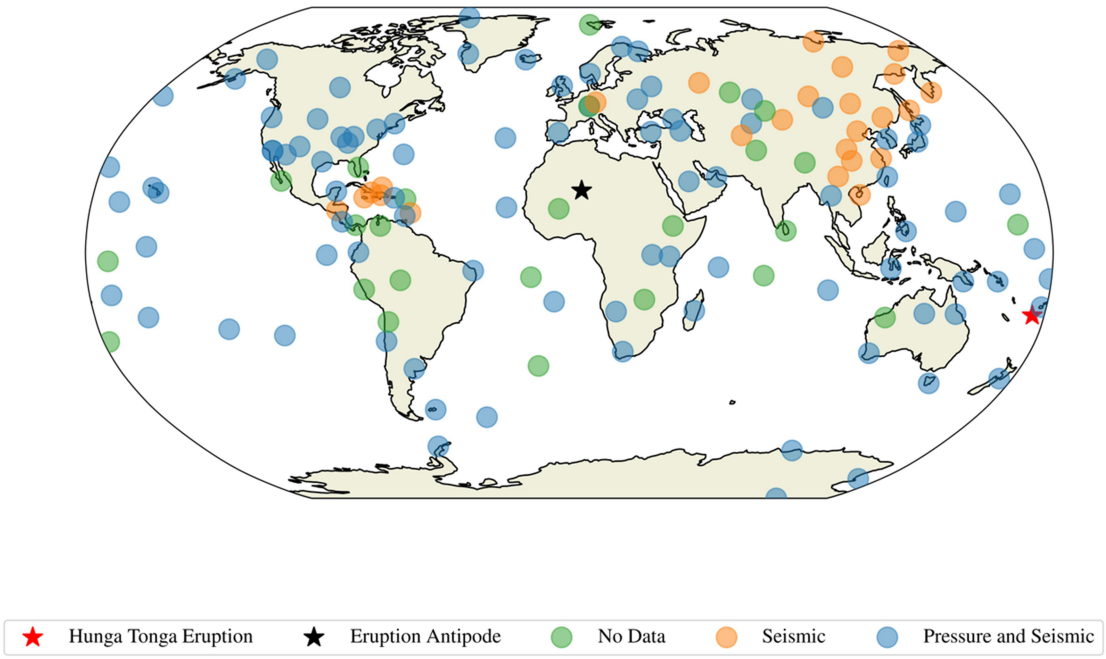

Figure 1: Map of the Global Seismographic Network (GSN) which includes the USGS Caribbean network (network code CU), the IRIS/IDA network (network code II), the IRIS/USGS network (network code IU), and the New China Digital Seismograph Network (network code IC; ASL, 1992). Stations from these networks that did not provide data (e.g., station was down) during the event are depicted by green circles. Stations with both a microbarograph and seismometer are depicted by blue circles. Stations with only a seismometer are depicted by orange circles. We have included the location of the Hunga Tonga eruption (red star) as well as the antipode (black star).

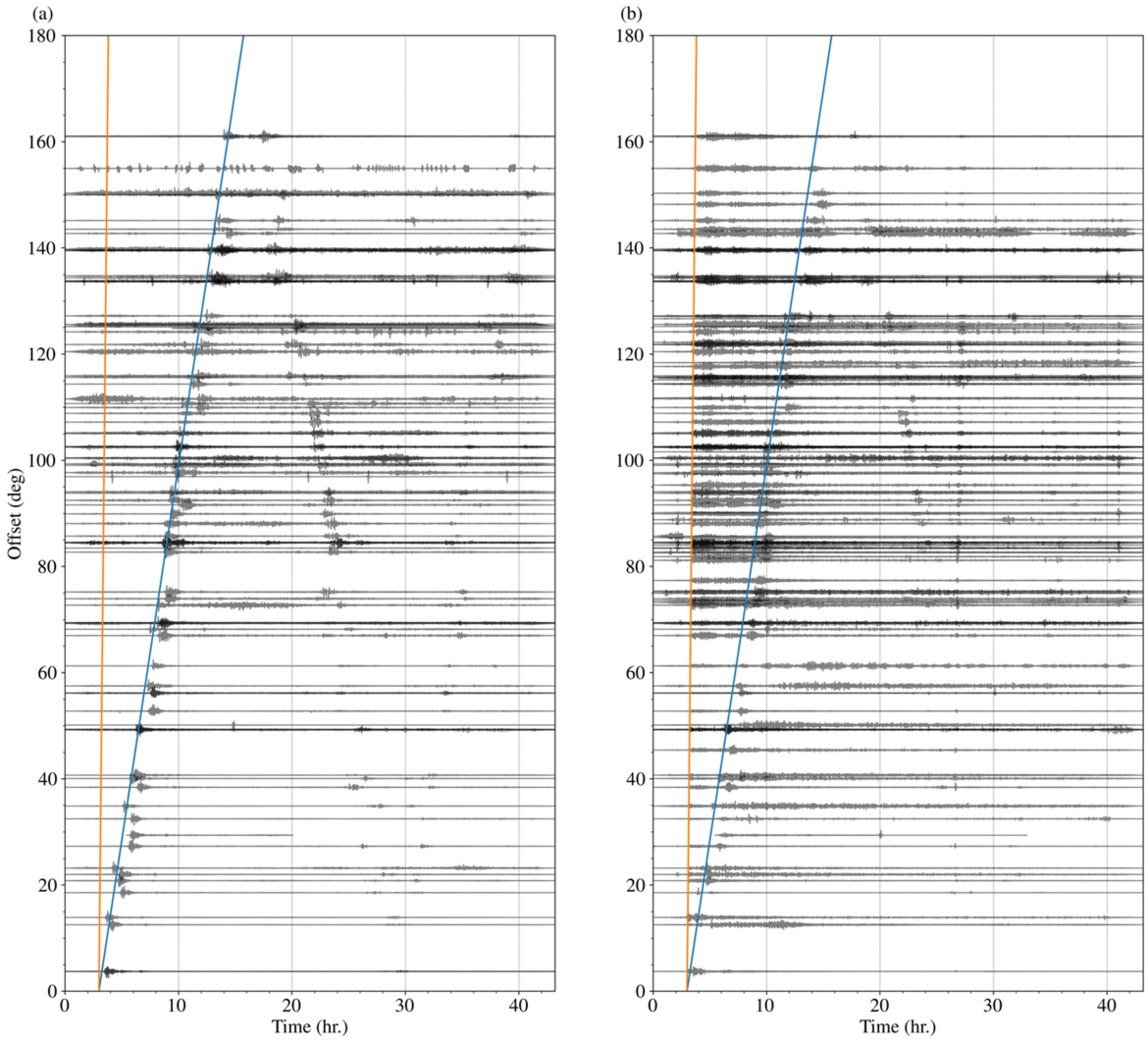

Figure 2: (a) Bandpass filtered record section from 100 mHz to 1 mHz of microbarographs (channel LDO) in the Global Seismographic Network (GSN) with a starting time of 00:00:00 January 15, 2022, UTC. (b) Same as (a), but for the long-period vertical component seismic data (channel LHZ). For reference we have included the predicted arrival time of a Lamb wave traveling at 310 m/s (blue) as well as a Rayleigh wave travelling at 4000 m/s (orange).

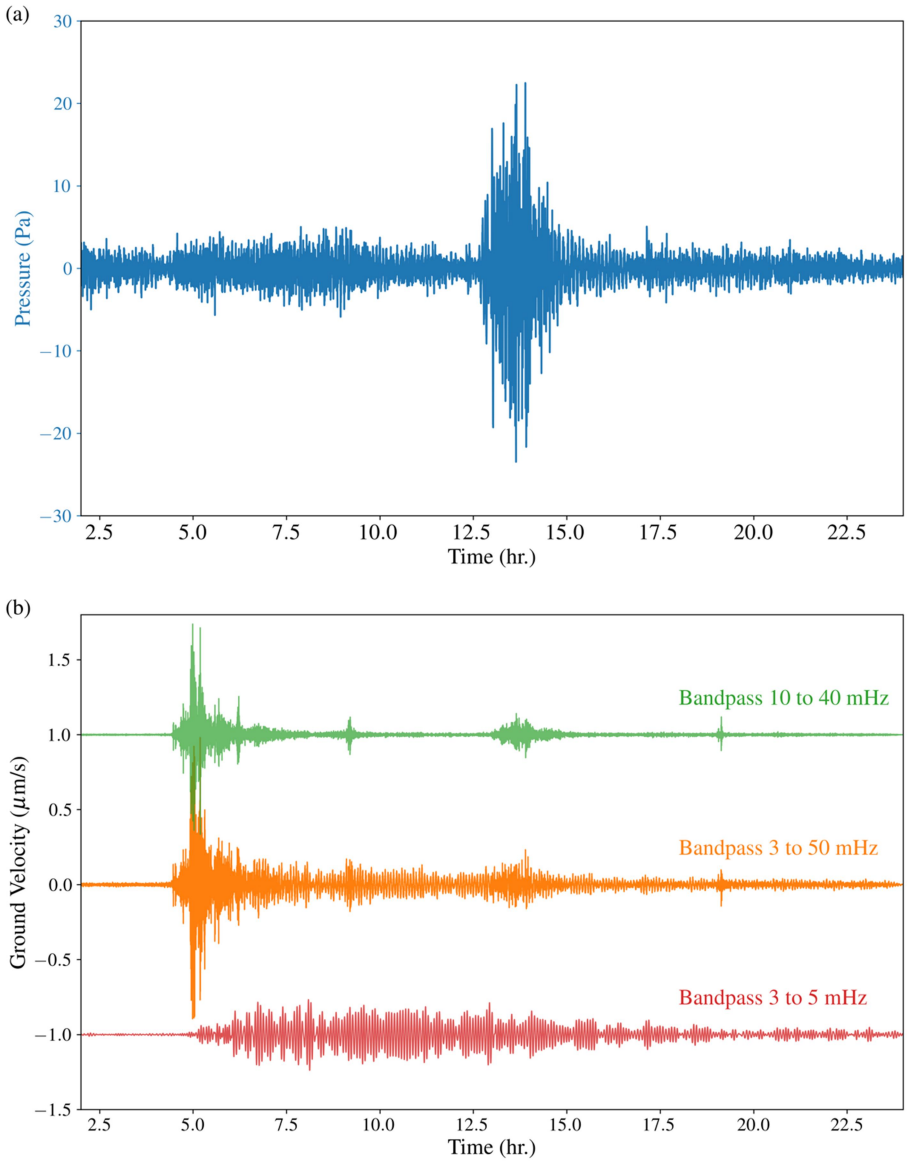

Figure 3: (a) Time series of pressure as recorded by the microbarograph at GSN station ANMO (Albuquerque, New Mexico; 9524 km from Hunga Tonga) after bandpass filtering from 3 to 50 mHz. The times are relative 00:00:00 January 15, 2022, UTC. (b) Time series of the vertical seismic records as recorded by the primary sensor (location code 00) at GSN station ANMO

after bandpass filtering from 10 to 40 mHz (green), 3 to 5 mHz (orange), and 3 to 5 mHz (red). All three traces are offset vertically on the plot for clarity.

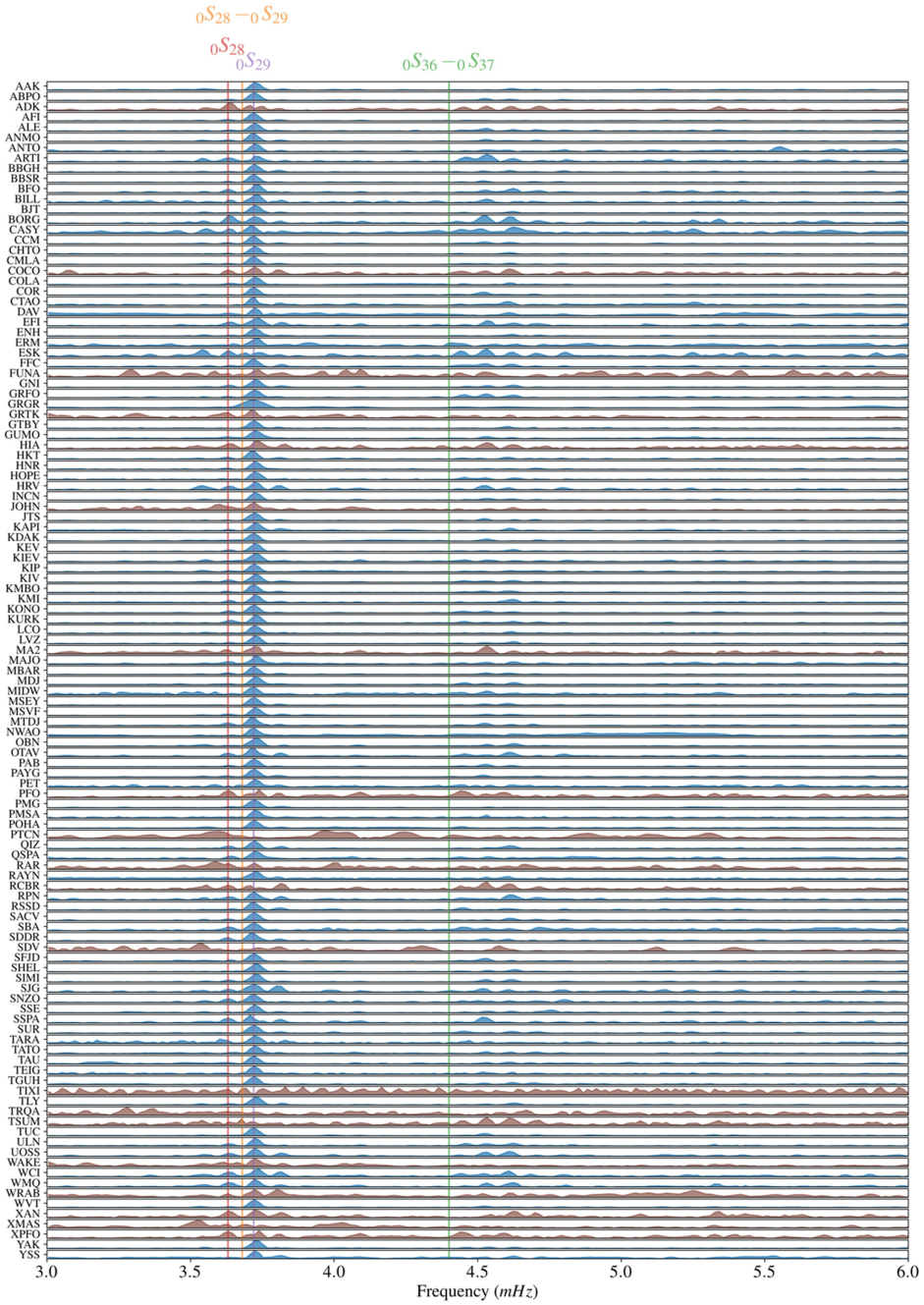

Figure 4: Vertical component spectra from 15 hours of data starting at 04:14:00 January 15, 2022, UTC for all primary (location code 00) seismometers (channel code LHZ) across the

Global Seismographic Network. Stations that recorded the 3.7 mHz signal with a signal-to-noise ratio (SNR) greater than 3 are shown in blue, while stations with a lower SNR are shown in brown. For reference we include the frequencies of ${}_0S_{28}$ (3.63 mHz, red) and ${}_0S_{29}$ (3.72 mHz, purple) as estimated by the Preliminary Reference Earth Model (PREM; Dziewonski and Anderson, 1981) as well as the atmospheric modes ${}_0S_{28}$-${}_0S_{29}$ (3.68 mHz, orange) and ${}_0S_{36}$-${}_0S_{37}$ (4.40 mHz, green) from Lognonné et al. (1998).

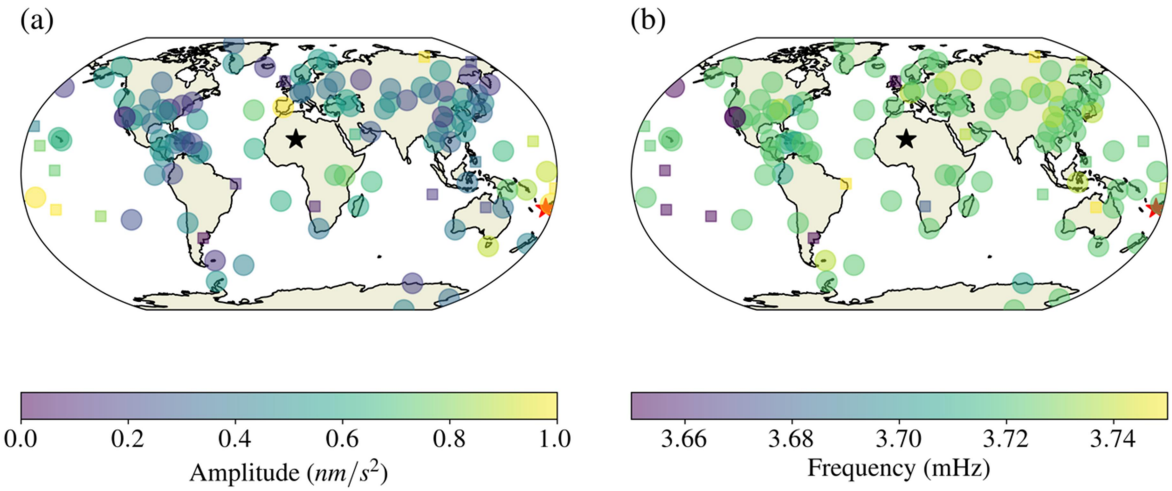

Figure 5: (a) Maximum amplitude of spectra in the 3.5 to 3.8 mHz band for 12 hours of data starting at 04:14:00 January 15, 2022, UTC for all primary (location code 00) seismometers (channel code LHZ) across the Global Seismographic Network. Stations with signal-to-noise ratio (SNR) greater than 3 are denoted by circles, and stations with an SNR less than 3 are denoted by squares. The location of the Hunga Tonga eruption is denoted by a red star, and the antipode is depicted by a black star. (b) Same as (a), but for the frequency where the peak amplitude occurred.

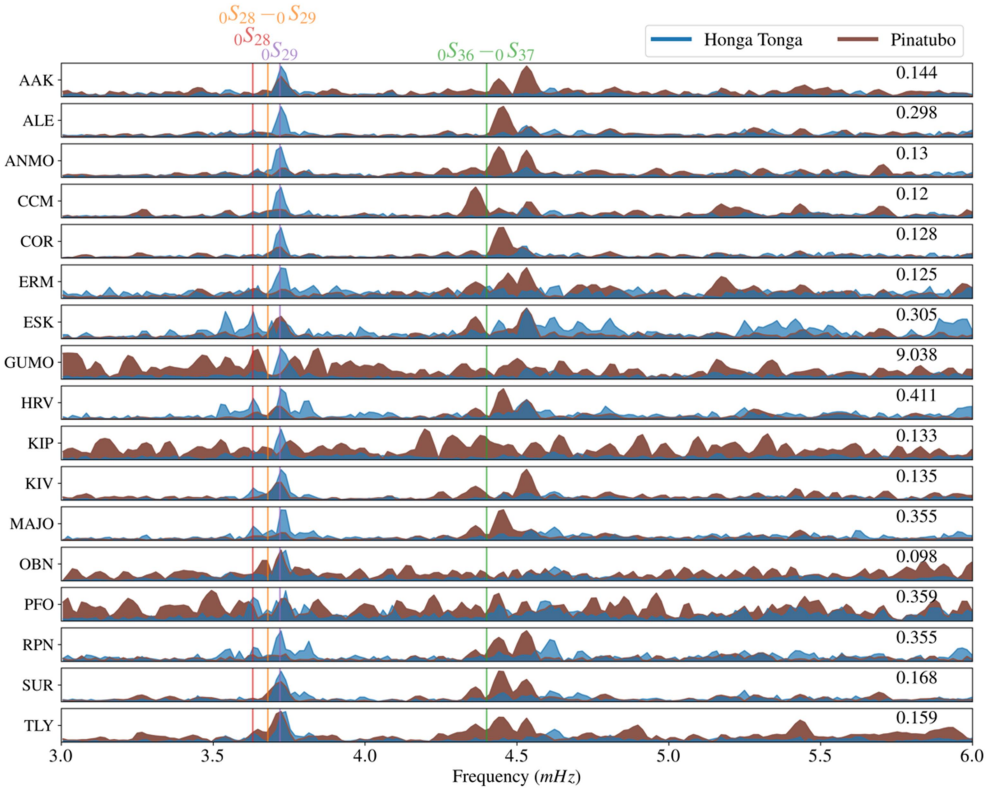

Figure 6: Vertical component spectra from 12 hours of data starting at 04:14:00 January 15, 2022 UTC for all primary (location code 00) seismometers (channel code LHZ) at 17 stations of the Global Seismographic Network (blue) and for the Pinatubo eruption starting at 06:30:00 June 15, 1991 (brown). Spectra were normalized to the peak amplitude in the 3 to 6 mHz frequency band. For reference we include the frequencies of $_0S_{28}$ (3.63 mHz, red) and $_0S_{29}$ (3.72 mHz, purple) as estimated by the Preliminary Reference Earth Model (PREM; Dziewonski and Anderson, 1988) as well as the atmospheric modes $_0S_{28}$-$_0S_{29}$ (3.68 mHz, orange) and $_0S_{36}$-$_0S_{37}$ (4.40 mHz, green) from Lognonné et al. (1998). The numbers on the right-hand side indicate the ratio of the peak amplitude of the Pinatubo event relative to the peak amplitude of the Hunga Tonga eruption in the 3 to 6 mHz frequency band.

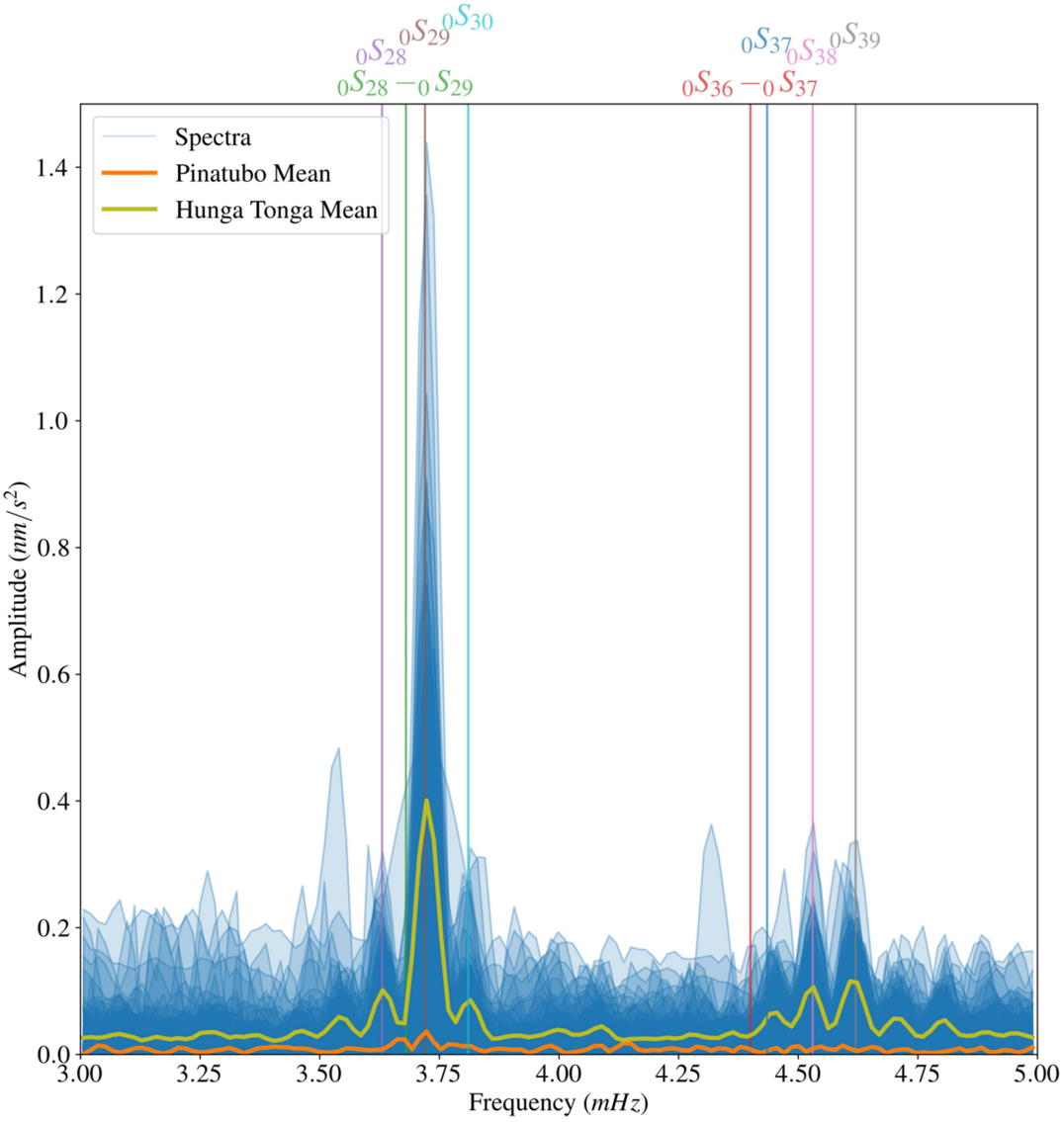

Figure 7: Vertical component spectra from 12 hours of data for the Hunga Tonga eruption starting at 04:14:00 January 15, 2022, UTC for all primary (location code 00) seismometers (channel code LHZ) across the Global Seismographic Network (blue) as well as the mean spectra of all stations for the Hunga Tonga event (green) and the Pinatubo event (orange). We have removed all spectra that had amplitudes greater than 0.6 nm/s^2 in the 3.9 to 4.1 mHz band and 0.35 nm/s^2 in the 3.0 to 3.4 mHz band because these are spectra that are dominated by noise. For

reference we include the frequencies of ${}_0S_{28}$ (3.63 mHz, purple), ${}_0S_{29}$ (3.72 mHz, brown), ${}_0S_{30}$ (3.81 mHz, cyan), ${}_0S_{37}$ (4.43 mHz, dark blue), ${}_0S_{38}$ (4.53 mHz, pink), and ${}_0S_{39}$ (4.62 mHz, grey) as estimated by the Preliminary Reference Earth Model (PREM; Dziewonski and Anderson, 1981) as well as the atmospheric modes ${}_0S_{28}$-${}_0S_{29}$ (3.68 mHz, green) and ${}_0S_{36}$-${}_0S_{37}$ (4.40 mHz, red) from Lognonné et al. (1998).

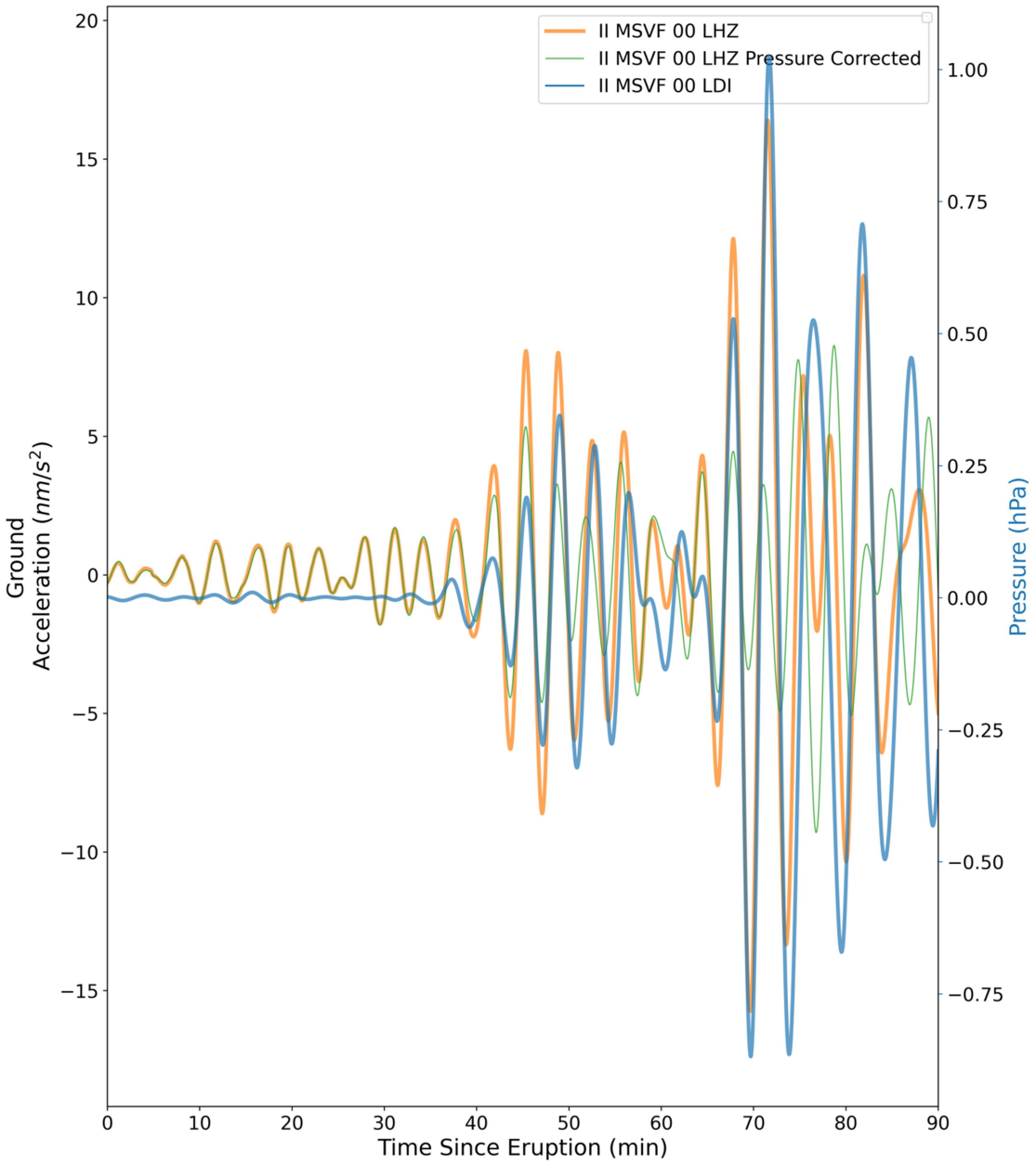

Figure 8: 90 minutes of time series data from IRIS/IDA station MSVF (Monasavu, Fiji) starting at 04:14:00 January 15, 2022, UTC for the microbarograph (channel: LDI, blue) and the vertical

component seismic data (channel: LHZ, orange) after filtering from 3 to 5 mHz. We also show the vertical seismic data after subtracting off a pressure correction coefficient of 13.3 nm/s^2/hPa that was estimated by minimizing the sum of the squares (green). This pressure corrected data has a variance reduction of 33% over the original acceleration data (orange).

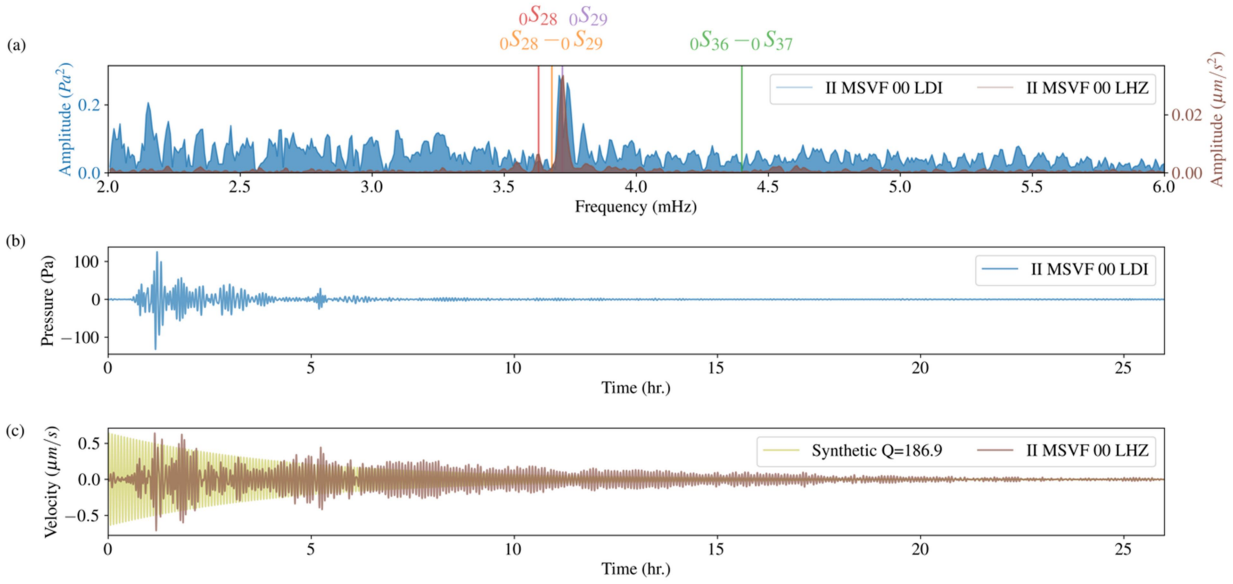

Figure 9: (a) Spectra for the microbarograph (blue) at IRIS/IDA station MSVF (Monasavu, Fiji) for 26 hours of data starting at 04:14:00 January 15, 2022, UTC. Spectra for the vertical component seismic data (brown) are also included. For reference we include the frequencies of $_0S_{28}$ (3.63 mHz, red) and $_0S_{29}$ (3.72 mHz, purple) as estimated by the Preliminary Reference Earth Model (PREM; Dziewonski and Anderson, 1981) as well as the atmospheric modes $_0S_{28}$-$_0S_{29}$ (3.68 mHz, orange) and $_0S_{36}$-$_0S_{37}$ (4.40 mHz, green) from Lognonné et al. (1998). (b) Time series for the pressure data used in after bandpass filtering between 2.5 and 5 mHz (a). (c) Time series for the seismic data (brown) used in part (a) as well a synthetic decaying sinusoid with a Q=186.9 (yellow) after bandpass filtering between 2.5 and 5 mHz.

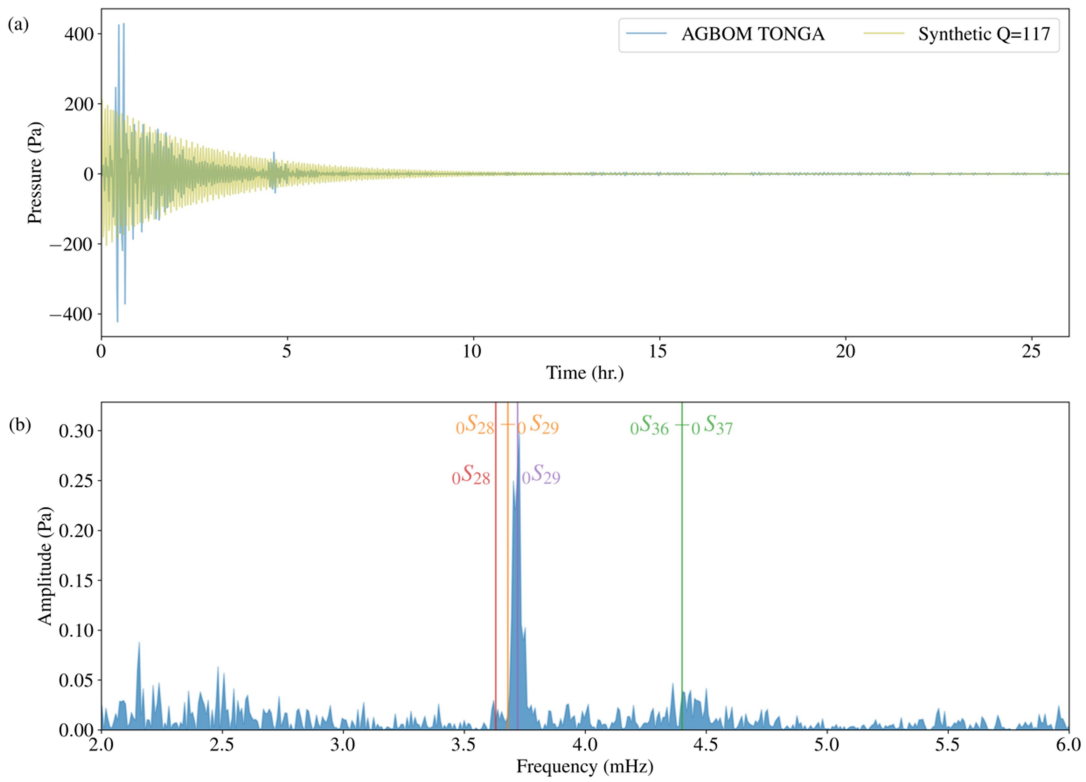

Figure 10: (a) 26 hours of time series of pressure data from the Australian Government Bureau of Meteorology (AGBOM) barometer located in Tonga (about 68 km from eruption, latitude -21.1303, longitude -175.1967, blue) starting at 04:14:00 January 15, 2022 UTC after bandpass filtering between 2.5 and 5 mHz. A synthetic decaying sinusoid with a Q=117 and a peak amplitude of one-half the maximum of the blue time series is shown in yellow. (b) Corresponding spectra from the time series in (a). For reference we include the frequencies of ${}_0S_{28}$ (3.63 mHz, red) and ${}_0S_{29}$ (3.72 mHz, purple) as estimated by the Preliminary Reference Earth Model (PREM; Dziewonski and Anderson, 1981) as well as the atmospheric modes ${}_0S_{28}$-${}_0S_{29}$ (3.68 mHz, orange) and ${}_0S_{36}$-${}_0S_{37}$ (4.40 mHz, green) from Lognonné et al. (1998).

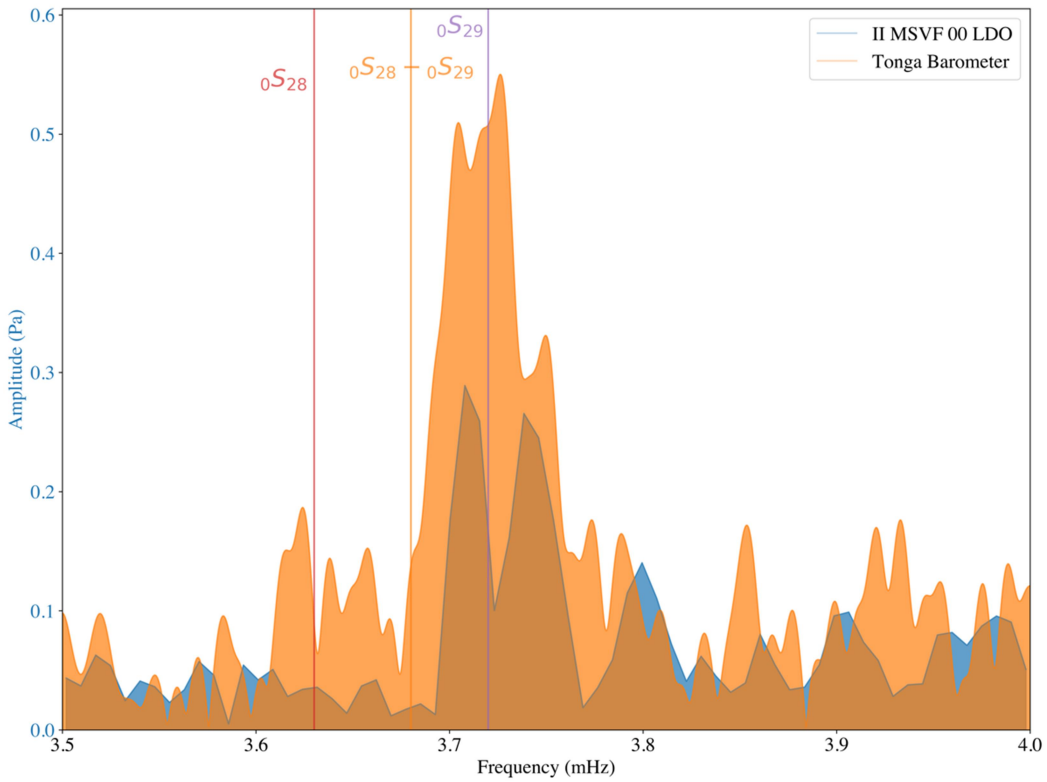

Figure 11: Spectra for the microbarograph (blue) at IRIS/IDA station MSVF (Monasavu, Fiji) for 26 hours of data starting at 04:14:00 January 15, 2022, UTC. Spectra from a barometer located in Tonga (about 68 km from eruption, latitude -21.1303, longitude -175.1967, orange) are also included. For reference we include the frequencies of $_0S_{28}$ (3.63 mHz, red) and $_0S_{29}$ (3.72 mHz, purple) as estimated by the preliminary reference Earth model (PREM; Dziewonski and Anderson, 1988) as well as the atmospheric mode $_0S_{28}$-$_0S_{29}$ (3.68 mHz, orange) from Lognonné et al. (1998).